

Precision Measurement of the Optical Conductivity of Atomically Thin Crystals via the Photonic Spin Hall Effect

Shizhen Chen, Xiaohui Ling, Weixing Shu, Hailu Luo^{*}, and Shuangchun Wen

Laboratory for Spin Photonics, School of Physics and Electronics, Hunan University, Changsha, 410082, China

(Received 4 September 2019; revised manuscript received 27 November 2019; published 29 January 2020)

How to measure the optical conductivity of atomically thin crystals is an important but challenging issue due to the weak light-matter interaction at the atomic scale. The photonic spin Hall effect, as a fundamental physical effect in light-matter interaction, is extremely sensitive to the optical conductivity of atomically thin crystals. Here we report a precision measurement of the optical conductivity of graphene, where the photonic spin Hall effect acts as a measurement pointer. By use of the weak-value-amplification technique, the optical conductivity of monolayer graphene taken as a universal constant of $(0.993 \pm 0.005)\sigma_0$ is detected, and a high measurement resolution of $1.5 \times 10^{-8} \Omega^{-1}$ is obtained. For few-layer graphene without a twist, we find that the conductivities increase linearly with the number of layers. Our idea could provide an important measurement technique for probing other parameters of atomically thin crystals, such as the magneto-optical constant, circular dichroism, and optical nonlinear coefficient.

DOI: [10.1103/PhysRevApplied.13.014057](https://doi.org/10.1103/PhysRevApplied.13.014057)

I. INTRODUCTION

Atomically thin crystals have extraordinary electronic and photonic properties that hold great promise in the applications of photonics and optoelectronics [1]. Characterization of the parameters of atomically thin crystals is therefore essential for photonic and optoelectronic applications. Graphene, a several-atomic-layer structural element of graphite, has attracted much attention due to its novel optical and electrical properties [2]. The optical properties of graphene, such as the remarkable absorption, reflectivity, and plasmonic response, are closely related to its optical conductivity [3–5]. In general, optical measurement extracts information from the measured system via light-matter interaction. Therefore, how to measure the optical conductivity of atomically thin crystals is still a challenging issue due to the weak light-matter interaction at the atomic scale.

There is some confusion about the actual value of the optical conductivity. Theoretical prediction has shown that the conductivity is generally frequency dependent [6]. At low photon energies, the conductivity is due to intraband transitions. However, it is argued that in the high-frequency range the optical conductivity should be a universal constant $\sigma_0 = e^2/4\hbar$ due to interband processes [7–9]. Optical spectroscopy measurements also yield a universal dynamic conductivity of $(1.01 \pm 0.04)\sigma_0$ over the visible-frequency range [10]. This approach can measure the optical conductivity with optical absorption in a wide spectral regime [11,12]. At lower photon energies a

departure from the universal constant has been observed. Another experimental measurement showed that the conductivity rises smoothly and steadily in the visible spectral range [13]. Therefore, it remains ambiguous whether the universal hypothesis holds for the optical conductivity at visible frequencies. Moreover, because of the weak interaction between graphene and light, an advanced measurement method and high measurement resolution are urgently needed.

In this paper, the photonic spin Hall effect (SHE) [14–17], as a fundamental physical effect in light-matter interaction, is proposed to realize the precision measurement of the optical conductivity of atomically thin crystals. The photonic SHE, including its underlying physics and possible applications, has been extensively studied in recent years [18,19]. This effect is attributed to the spin-orbit coupling during the process of light-matter interaction. The photonic SHE manifested as a spin-dependent shift provides important information on an optical interface [20], and therefore it can be used as a pointer in precision measurements. The photonic SHE is a weak effect whose initial shift is only a fraction of a wavelength, and therefore it cannot be detected directly by conventional optical measurements. By use of weak-value-amplification techniques [21], however, the initial shift can be enhanced by nearly 4 orders of magnitude [22]. A sensitivity of 1 Å to observe the photonic SHE has been achieved.

II. THEORETICAL DESCRIPTION

The general model treats an atomically thin crystal as a homogeneous slab with an effective thickness and a certain

*hailuluo@hnu.edu.cn

refractive index [23–26]. However, for a truly atomic crystal whose thickness is much less than the wavelength of light, the refractive index seems not well defined. It has been shown that the model with zero thickness can more accurately describe the optical response of graphene [27]. This zero-thickness model is well established by considering atomically thin crystals as a two-dimensional conductive film characterized by the surface parameters.

Let us consider that an electromagnetic wave propagating in a dielectric medium with refractive index n_1 impinges on a flat interface with a second medium with refractive index n_2 , which is coated with a few-layer atomic crystal. In the two media, the electric (magnetic) fields are represented by \mathbf{E}_1 and \mathbf{E}_2 (\mathbf{H}_1 and \mathbf{H}_2), respectively. \mathbf{E} is related to \mathbf{H} in a vacuum by the impedance Z_0 of the vacuum. If we take the surface current density into account, the boundary conditions are $\hat{\mathbf{n}} \times (\mathbf{E}_2 - \mathbf{E}_1) = 0$ and $\hat{\mathbf{n}} \times (\mathbf{H}_2 - \mathbf{H}_1) = \mathbf{J}_s + \mathbf{J}_p$, where $\hat{\mathbf{n}} = -\hat{\mathbf{z}}$ is the unit vector normal to the interface, $\mathbf{J}_s = \sigma \mathbf{E}$ is from Ohm's law, where σ is the optical conductivity of the atomically thin crystal, and $\mathbf{J}_p = \partial \mathbf{P} / \partial t$ is a current density that depends on the change of polarization $\mathbf{P} = \varepsilon_0 \chi \mathbf{E}$, with ε_0 and χ being the permittivity and electric susceptibility, respectively. On the basis of the boundary condition, the Fresnel coefficients can be obtained [28–30] (see Appendix A). If σ and χ are both zero, the Fresnel coefficients reduce to the ordinary forms at an air-glass interface.

When a light beam impinges on the surface of graphene, it experiences the photonic SHE shown as a tiny separation of two spin components in Fig. 1. A bounded beam can be regarded as the combination of plane electromagnetic waves. As the photonic SHE appears in the y direction, we consider only the wave-vector k_y component in the momentum space. If the polarization of the beam is horizontal, the polarization states of different angular-spectrum components can be written as $|H(k_y)\rangle$.

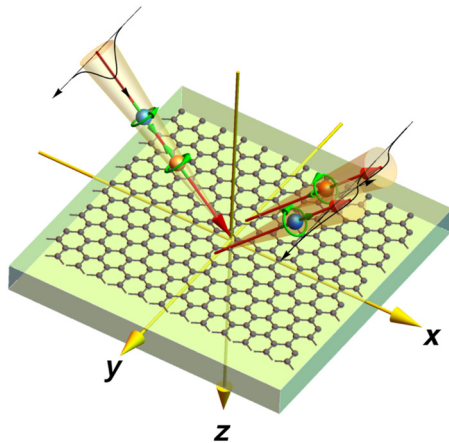


FIG. 1. Photonic spin Hall effect at an air-graphene interface. The reflected light beam experiences a spin-dependent shift due to the spin-orbit coupling on the surface of graphene.

The polarization of each angular-spectrum component is related to the reflection coefficients dependent on wave vector. After reflection at the graphene interface, the rotations of the polarizations for each angular-spectrum component are different to satisfy the photon transversality. Under the paraxial approximation, the change in the polarization state after reflection becomes

$$|H(k_y)\rangle \rightarrow r_p |H(k_y)\rangle - \frac{k_y \cot \theta_i (r_p + r_s)}{k_0} |V(k_y)\rangle, \quad (1)$$

where $k_0 = \omega/c$ is the wave vector in a vacuum, θ_i is the angle of incidence, and $|V(k_y)\rangle$ is the vertical polarization caused by a tiny rotation of the polarization, which originates from the spin-orbit coupling of light.

To interpret the spin-orbit coupling more clearly, the state can be written in the spin basis as the relations $|H\rangle = \frac{1}{\sqrt{2}}(|+\rangle + |-\rangle)$ and $|V\rangle = \frac{1}{\sqrt{2}}i(|-\rangle - |+\rangle)$. Under the condition of weak interaction $k_y \delta \ll 1$, Eq. (1) becomes

$$|H(k_y)\rangle \rightarrow \exp(-k_y \delta)|+\rangle + \exp(k_y \delta)|-\rangle, \quad (2)$$

where δ represents the spin-dependent shift induced by the spin-orbit interaction,

$$\delta = [(r_p + r_s) \cot \theta_i]/(k_0 r_p). \quad (3)$$

The spin-dependent shift is determined by the Fresnel coefficients, and is related to the optical conductivity. Therefore, the photonic SHE can serve as a pointer in measurements of the optical conductivity of atomically thin crystals. The wave function in the spin basis $|s\rangle$ ($s = \pm 1$) can be written as $|\psi\rangle = \int \exp(-k_y \hat{\sigma}_3 \delta) |\Phi(k_y)\rangle |s\rangle dk_y$, with $|\Phi(k_y)\rangle$ being a Gaussian distribution. Here $\exp(-k_y \hat{\sigma}_3 \delta)$ indicates the spin-orbit coupling of light, with $\hat{\sigma}_3$ being the Pauli operator. By use of weak-value-amplification techniques, the shift as well as the optical conductivity can be precisely measured.

In a weak-measurement scheme, the coupling between the observable and the meter is weak, and only a small amount of information is extracted [31,32]. Here the observable is the spin of the photon and the spin-dependent shifts serve as the pointer of the meter. In the linear theory with approximation, the output of the weak measurement is an extraordinary value called the “weak value.” The weak value is naturally determined by the preselected state $|\psi_i\rangle$ and the postselected state $|\psi_f\rangle$, and is given by

$$A_w = \frac{\langle \psi_f | \hat{\sigma}_3 | \psi_i \rangle}{\langle \psi_f | \psi_i \rangle} \quad (4)$$

(see Appendix B). A large weak value can be obtained when the preselected state and the postselected state are close to orthogonal, $\langle \psi_f | \psi_i \rangle \approx 0$.

We choose the preselected state as $|H\rangle = (|+\rangle + |-\rangle)/\sqrt{2}$ in our measurement. To achieve a large weak value, the postselected state $|\psi_f\rangle$ needs to be nearly orthogonal to $|\psi_i\rangle$. That is, $|\psi_f\rangle = \sin(\pi/4 + \alpha)|+\rangle - e^{2i\beta}\cos(\pi/4 + \alpha)|-\rangle$, with α and β being the small deviation angles as shown on the Poincaré sphere in Fig. 2(a). From the above preselected and postselection states, the weak value A_w of the observable $\hat{\sigma}_3$ is a complex number [33,34]. The wave function after the preselected and postselected ensembles becomes $\langle\psi_f|\psi\rangle = \int \exp(-k_y A_w \delta) |\Phi(k_y)\rangle dk_y$ (see Appendix B). The real and imaginary parts of the weak value are related to the angles α and β , which amplify the spin-dependent shifts as shown in Fig. 2(b). The spin-dependent shifts in the photonic SHE serve as a pointer, and the imaginary part of the weak value would be significantly amplified due to the free evolution of the wave function. In our experiment, a purely imaginary weak value is obtained as $A_w = i \cot \beta$ with $\alpha = 0$.

In our case, the free-evolution factor F is related to the meter state for the wave-function evolution in the real position space [35,36]. The factor given by $F = z/z_r$ together with the weak value amplify the initial pointer shift, where $z = 250$ mm is the effective evolution distance. In the linear theory of weak measurements [21], the final amplified pointer shift is given by

$$\langle y \rangle = F \text{Im}(A_w) \delta = \frac{z}{z_r} \cot \beta \delta. \quad (5)$$

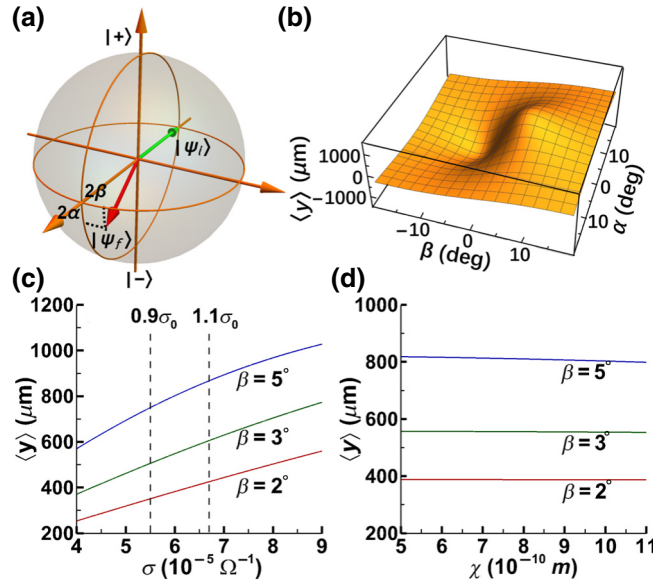


FIG. 2. Amplification of the photonic spin Hall effect with pre-selected and postselected ensembles. (a) Representation of the initial and final states on the Poincaré sphere. (b) Amplification of spin-dependent splitting as a function of the angles α and β . The amplified shifts vary with (c) optical conductivity and (d) electric susceptibility. The dashed line indicates the conductivity corresponding to $0.9\sigma_0$ and $1.1\sigma_0$.

From Eq. (5), we can achieve an amplified pointer shift about $F \cot \beta$ times larger than the initial pointer shift. Equation (5) is the simplest form that can explain the underlying physics of weak measurements clearly. However, it would fail to describe the weak-value amplification for small postselected angle β . The strict expression of the amplified pointer shift can be obtained as

$$\langle y \rangle = \frac{z r_p (r'_p + r'_s) \cot \theta_i \sin 2\beta}{(r'_p + r'_s)^2 \cos^2 \beta \cot^2 \theta_i + [2k_0 z_r (r'^2_p + r'^2_s) + \xi^2] \sin^2 \beta}, \quad (6)$$

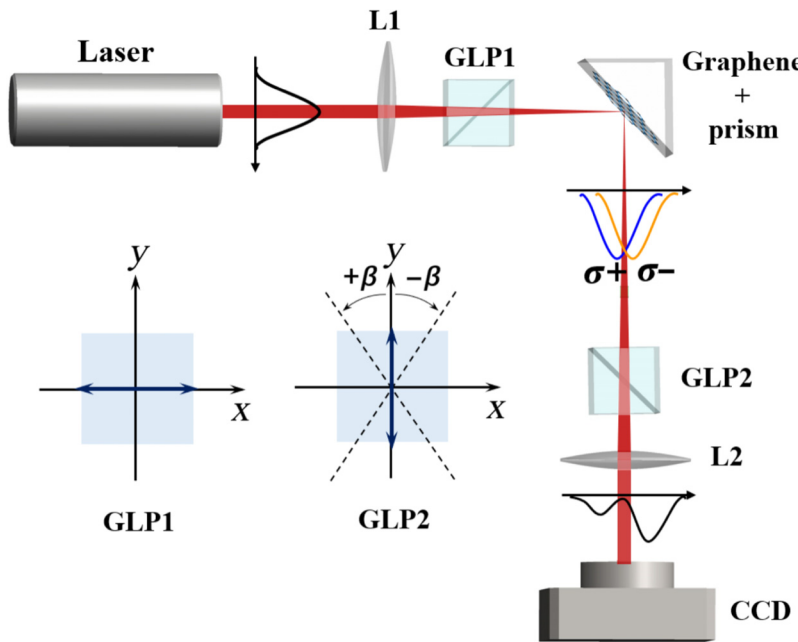
where $\xi = \text{Re}(\partial r_p / \partial \theta_i)$ from the Taylor-series expansion, and the complex reflectance coefficients are defined as $r_p = r'_p + ir''_p$ and $r_s = r'_s + ir''_s$. The detailed calculation is given in Appendix B.

To demonstrate the sensitivity of the photonic SHE to the optical conductivity, the results of the calculation with Eq. (6) with change of the conductivity of monolayer graphene are shown in Fig. 2(c). The incident angle θ_i is chosen as 56.6° . At this angle, the spin-orbit interaction in the photonic SHE is strong and thus increases the sensitivity to the optical conductivity [37]. For $\beta = 2^\circ, 3^\circ$, and 5° , amplified factors $F \cot \beta \approx 3200, 2140$, and 1280 are obtained with Rayleigh length $z_r \approx 2.23$ mm. Another important parameter (susceptibility χ) in graphene may also have an influence on the photonic SHE due to the change of polarization with time in atomic sheets. Merano [27] used the experimental data to fit the susceptibility as $(8 \pm 3) \times 10^{-10}$ in the visible spectral range [38]. The pointer shifts with variation of χ from 5×10^{-10} to 11×10^{-10} m are given in Fig. 2(d). It is seen that the contribution of the susceptibility to the amplified pointer shifts can be ignored.

In previous work, the slab model with effective thickness was used to describe the photonic SHE in graphene [25]. However, this model may be inexact under some conditions, such as with $\beta \gtrsim 5^\circ$ here. Merano [27] verified that the zero-thickness model may be a better choice. In our experiment, to precisely measure the conductivity, we need to detect the photonic SHE with the variation of β from 0° to 5° or more. This is because the data with larger β are more effective and stabler to determine the optical conductivity, which is discussed in the following section.

III. EXPERIMENTAL MEASUREMENT AND DISCUSSION

Our graphene sample is supported on bulk SiO₂ glass substrates (standard BK7, Thorlabs PS911). The clean SiO₂ substrate is directly covered with monolayer, bilayer, or trilayer Trivial Transfer Graphene by chemical vapor deposition. The area of the region containing graphene is about 1 cm². In the work reported in Refs. [10,11], graphene supported on bulk SiO₂ substrate or suspended by a metal scaffold was prepared by mechanical exfoliation



of graphite. The measured area of the samples was only about several-hundred square micrometers.

The experimental setup to observe the photonic SHE is shown in Fig. 3. Our experiment is implemented in a dark room and the optical conductivity of the sample is detected at room temperature. A polarized Gaussian beam generated by a 17-mW linearly polarized He-Ne laser at 632.8 nm (Thorlabs HRP170) is reflected by a graphene-SiO₂ interface to produce the photonic SHE. The beam waist of the light beam after lens L1 is 21.2 μm . The spin displacements are much smaller than the width of the beam, so the meter states of different spin eigenstates almost overlap with each other. This provides the weak interaction in weak measurements, which is associated with the optical conductivity. In our system a purely imaginary weak value can result in a larger amplified factor due to effective light propagation. We use Glan laser polarizer GLP1 to preselect the initial state $|\psi_i\rangle$ and Glan laser polarizer GLP2 to postselect the final state $|\psi_f\rangle$ to obtain the purely imaginary weak value. The rotations of GLP2 corresponding to the projection of the states on the Poincaré sphere are shown in Fig. 2(a). After the postselection, the meter distribution with large displacement can be observed by a CCD camera (Coherent Laser-Cam HR).

The amplified pointer shift is measured with the rotation angle of GLP2 from 0° to 5°. We fabricate the samples with monolayer, bilayer, and trilayer graphene. Each graphene sample is illuminated with a light beam at three different incidence positions. The three groups of data for monolayer graphene represented by symbols with error bars in Fig. 4. We obtain the corresponding fitting curves to characterize the optical conductivity from the experimental pointer shifts. In Ref. [27], the

FIG. 3. Experimental setup to detect the tiny spin-orbit interaction of light in graphene. A polarized Gaussian beam generated by a He-Ne laser is incident at an angle on the graphene interface. Lenses L1 and L2 focus and collimate the light beam. The Glan laser polarizers (GLP1 and GLP2) select the preselected and postselected states, respectively. The CCD camera is used to capture the intensity profiles.

ensemble of the experimental data extracted from some remarkable experiments can fit an optical conductivity of $(1.00 \pm 0.33)\sigma_0$ for the spectral range from 450 to 750 nm. An optical conductivity of $(1.0 \pm 0.1)\sigma_0$ was obtained by observing the frequency-independent absorbance of graphene in Ref. [11]. To show the measurement accuracy of our method, the theoretical curves of amplified shifts for optical conductivity of $0.67\sigma_0$, $0.9\sigma_0$, $1.1\sigma_0$, and $1.33\sigma_0$

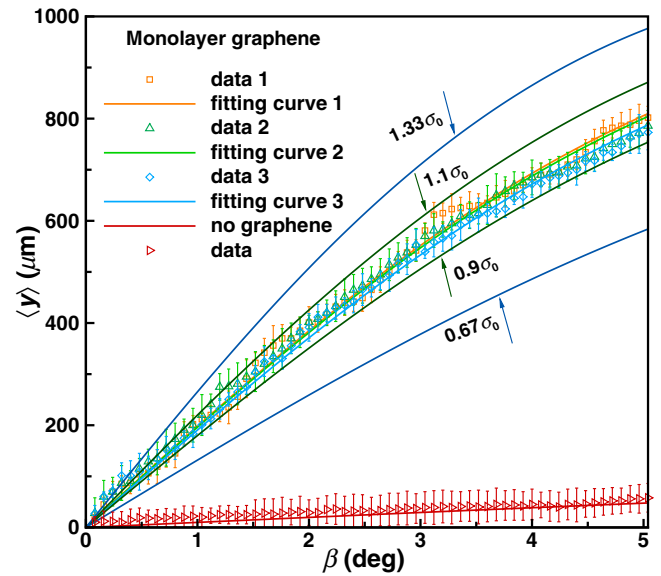


FIG. 4. Amplification of pointer shifts as a function of the postselected angle β . Theoretical results for optical conductivity taken as $0.67\sigma_0$, $0.9\sigma_0$, $1.1\sigma_0$, and $1.33\sigma_0$. The fitting curves are obtained on the basis of three groups of data. For comparison, the result without graphene is also given.

are given. The CCD we use has a displacement resolution of $1 \mu\text{m}$. On the basis of Eq. (5) with $\beta = 2^\circ$, this leads to the minimum resolution of optical conductivity being $1.5 \times 10^{-8} \Omega^{-1}$. By fitting curves extracted from weak measurements, we can achieve a high resolution of about $\pm 0.005\sigma_0$ with our method.

From the well-established theoretical model, the real part of the optical conductivity of monolayer graphene is a steplike function of frequency at zero temperature, and there is no imaginary part in the high-frequency region [39]. The environment, such as the temperature and the chemical potential, affects conductivity only near the step-like point. For monolayer graphene, the bottom horizontal black line in Fig. 5 indicates the conductivity with a universal-constant value. The horizontal green lines correspond to the values $0.9\sigma_0$ and $1.1\sigma_0$ to highlight our measurement accuracy. It is shown that the deviation of the experimental results becomes smaller when the measured angle β is large enough. This is due to the amplified shifts being indistinguishable at small β , as shown in Fig. 4. In the detection of the photonic SHE, enough photons need to be collected by the CCD to resolve the position of the beam distribution. The measurement accuracy of the shift can be limited by some factors, such as the laser-pointing stability or misaligned optical elements. Because of the existence of faint background noise, the lack of intensity saturation in the CCD may lead to an unwanted tiny deviation of the shift.

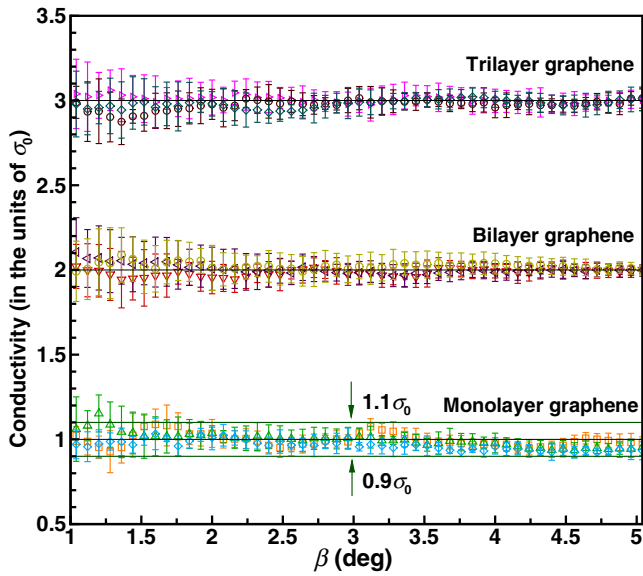


FIG. 5. Measurement of the optical conductivity in the unit of σ_0 for monolayer, bilayer, and trilayer graphene. Theoretically, the optical conductivity of monolayer graphene is taken as the universal constant $\sigma_0 = e^2/4\hbar$, shown as the bottom horizontal black line. The horizontal green lines correspond to the values $0.9\sigma_0$ and $1.1\sigma_0$. In addition, the optical conductivities of bilayer and trilayer graphene without a twist are also obtained.

For few-layer graphene without a twist, the results in Fig. 5 show that the conductivities of bilayer and trilayer graphene are close to $2\sigma_0$ and $3\sigma_0$, respectively. With appropriate angles of incidence, the measurement accuracy is still very high for few-layer graphene. The corresponding measurements of amplified pointer shifts are provided in Appendix C. In addition to the experiment measuring the optical conductivity described above, Raman spectra with the Raman peak to confirm the regions of monolayer, bilayer, and trilayer graphene are measured (see Appendix C).

IV. CONCLUSIONS

In conclusion, the optical conductivity of graphene is precisely measured on the basis of the photonic SHE and use of the weak-value-amplification technique. In our method, the spin-dependent shifts in the photonic SHE serve as a measurement pointer, and the weak-value-amplification technique is used to obtain an amplified pointer shift. The experimental results show that the optical conductivity of monolayer graphene is close to the universal-constant value $(0.993 \pm 0.005)\sigma_0$ with high measurement resolution of $1.5 \times 10^{-8} \Omega^{-1}$. Such high accuracy may result in application in the measurement of the tiny deviation from universal conductivity due to many-body effects [40]. For bilayer and trilayer graphene, the twist between the atomic sheets is not considered in our case. We find that the optical conductivity of few-layer graphene increases linearly with the number of layers. It would be very interesting to measure the optical conductivity of suspended graphene, chiral graphene [41], and magic angle graphene [42,43].

ACKNOWLEDGMENTS

This work was supported by the National Natural Science Foundation of China (Grant No. 61835004) and the Fundamental Research Funds for the Central Universities (Grant No. 531118010313).

APPENDIX A: CALCULATION OF THE FRESNEL COEFFICIENTS

To obtain the reflection coefficients at an air-crystal interface, the boundary conditions for an electromagnetic field are considered. The electric (magnetic) fields in air and the substrate are represented by \mathbf{E}_1 and \mathbf{E}_2 (\mathbf{H}_1 and \mathbf{H}_2), respectively. Electric current should be taken into account. The boundary conditions are $\hat{\mathbf{n}} \times (\mathbf{E}_2 - \mathbf{E}_1) = 0$ and $\hat{\mathbf{n}} \times (\mathbf{H}_2 - \mathbf{H}_1) = \mathbf{J}_s + \mathbf{J}_p$, where $\hat{\mathbf{n}} = -\hat{\mathbf{z}}$ is the unit vector normal to the interface, \mathbf{J} has contributions from two parts, one is obtained from Ohm's law $\mathbf{J}_s = \sigma \mathbf{E}$, and the other \mathbf{J}_p is the current density with the change of polarization $\mathbf{P} = \varepsilon_0 \chi \mathbf{E}$ [27], where σ is the optical conductivity of the atomically thin crystal and ε_0 and χ are the

permittivity and electric susceptibility, respectively. For polarization state $|V\rangle$ ($|H\rangle$), we have

$$\mathbf{E}_{xi} + \mathbf{E}_{xr} = \mathbf{E}_{xt} \quad (\mathbf{E}_{yi} - \mathbf{E}_{yr} = \mathbf{E}_{yt}), \quad (\text{A1})$$

$$i\omega \mathbf{P}_x = \mathbf{J}_{px} \quad (i\omega \mathbf{P}_y = \mathbf{J}_{py}), \quad (\text{A2})$$

$$\sigma \mathbf{E}_{xt} = \mathbf{J}_{sx} \quad (\sigma \mathbf{E}_{yt} = \mathbf{J}_{sy}), \quad (\text{A3})$$

$$\begin{aligned} \mathbf{H}_{yi} - \mathbf{H}_{yr} &= \mathbf{H}_{yt} + \mathbf{J}_{px} + \mathbf{J}_{sx} \quad (\mathbf{H}_{xi} + \mathbf{H}_{xr} \\ &= \mathbf{H}_{xt} + \mathbf{J}_{py} + \mathbf{J}_{sy}), \end{aligned} \quad (\text{A4})$$

where ω is the angular frequency of the light. Solving Eqs. (A1)–(A4) with $Z_0 \mathbf{H}_{1(2)}/n_{1(2)} = \mathbf{E}_{1(2)}$, we obtain the reflection coefficients $r_s = \mathbf{E}_r/\mathbf{E}_i$ and $r_p = \mathbf{H}_r/\mathbf{H}_i$ as

$$r_s = \frac{n_1 \cos \theta_i - n_2 \cos \theta_t - ik\chi - \sigma Z_0}{n_1 \cos \theta_i + n_2 \cos \theta_t + ik\chi + \sigma Z_0}, \quad (\text{A5})$$

$$r_p = \frac{n_2 \cos \theta_i - n_1 \cos \theta_t + (ik\chi + \sigma Z_0) \cos \theta_i \cos \theta_t}{n_2 \cos \theta_i + n_1 \cos \theta_t + (ik\chi + \sigma Z_0) \cos \theta_i \cos \theta_t}, \quad (\text{A6})$$

where Z_0 is the impedance of a vacuum. Different plane-wave components experience tiny polarization rotations to satisfy transversality. The tiny rotations ultimately lead to the separation of left-circular and right-circular polarization.

APPENDIX B: CALCULATION OF THE OBSERVATION OF PHOTONIC SHE VIA WEAK MEASUREMENTS

The separation of left-circular and right-circular polarization in the photonic SHE is on the subwavelength scale. Use of weak-measurement-amplification technology is an effective method to observe it. To discuss the theory of weak measurements, we begin with the state after reflection evolution described by Eq. (3). The polarization of $|H\rangle$ or $|V\rangle$ can be decomposed into two orthogonal polarization components with relations $|H\rangle = i(|-\rangle - |+\rangle)/\sqrt{2}$ and $|V\rangle = (|+\rangle - i|-\rangle)/\sqrt{2}$, where $|+\rangle$ and $|-\rangle$ represent the left-circularly-polarized and right-circularly-polarized components, respectively. The wave function in momentum space can be specified by the following expression:

$$|\Phi\rangle = \frac{w_0}{\sqrt{2\pi}} \exp\left(-\frac{w_0^2(k_x^2 + k_y^2)}{4}\right), \quad (\text{B1})$$

where w_0 is the width of the wave function.

For $|H\rangle$ input polarization, the reflected wave function $|\varphi\rangle$ in the momentum space can be obtained as

$$\begin{aligned} |\varphi\rangle &= r_p |H\rangle - \frac{k_y(r_p + r_s) \cot \theta_i}{k_0} |V\rangle \\ &= \frac{r_p}{\sqrt{2}} [(1 + ik_y\delta)|+\rangle + (1 - ik_y\delta)|-\rangle] \\ &\approx \frac{r_p}{\sqrt{2}} [\exp(ik_y\delta)|+\rangle + \exp(-ik_y\delta)|-\rangle]. \end{aligned} \quad (\text{B2})$$

We have $|ik_y\delta| \ll 1$ since the spin-orbit interaction is weak at the interface reflection. With the Pauli operator $\hat{\sigma}_3$, the spin separation can be denoted by the spin-orbit-coupling term $\exp(i\hat{\sigma}_3 k_y \delta)$.

After the preselection of state $|\psi_i\rangle$, weak interaction, and the postselection of state $|\psi_f\rangle$, the wave function evolves to the final state:

$$\begin{aligned} |\Phi_f\rangle &= \langle \psi_f | \exp(i\hat{\sigma}_3 k_y \delta) | \psi_i \rangle |\Phi\rangle \\ &= \langle \psi_f | 1 + i\hat{\sigma}_3 k_y \delta | \psi_i \rangle |\Phi\rangle \\ &\approx \langle \psi_f | \psi_i \rangle \left(1 + ik_y \delta \frac{\langle \psi_f | \hat{\sigma}_3 | \psi_i \rangle}{\langle \psi_f | \psi_i \rangle} \right) |\Phi\rangle \\ &= \langle \psi_f | \psi_i \rangle (1 + ik_y A_w \delta) |\Phi\rangle. \end{aligned} \quad (\text{B3})$$

Here A_w is the so-called weak value and is given by

$$A_w = \frac{\langle \psi_f | \hat{\sigma}_3 | \psi_i \rangle}{\langle \psi_f | \psi_i \rangle}. \quad (\text{B4})$$

With the preselected state $|\psi_i\rangle = (|+\rangle + |-\rangle)/\sqrt{2}$ and the postselected state $|\psi_f\rangle = \sin(\pi/4 + \alpha)|+\rangle - e^{2i\beta} \cos(\pi/4 + \alpha)|-\rangle$, the weak value is obtained as

$$\text{Re } A_w = \frac{\sin 2\alpha}{2|\langle \psi_f | \psi_i \rangle|^2}, \quad \text{Im } A_w = -\frac{\cos 2\alpha \sin 2\beta}{2|\langle \psi_f | \psi_i \rangle|^2}, \quad (\text{B5})$$

where $|\langle \psi_f | \psi_i \rangle|^2 = \cos^2 \beta \sin^2 \alpha + \cos^2 \alpha \sin^2 \beta$. To obtain a purely imaginary weak value, we set $\alpha = 0$ in our experiment, and $A_w = i \cot \beta$.

We see that in the linear theory of weak measurements above, the weak value is obtained with strict conditions. However, in the experiment involving the photonic SHE, if the preselected and postselected states are nearly orthogonal, $\langle \psi_f | \psi_i \rangle \rightarrow 0$, A_w becomes an infinite number and is meaningless. On the other hand, when the angle of incidence is near the Brewster angle, the weak-interaction condition is invalid due to strong spin-orbit coupling of light. Therefore, the weak value A_w in the detection of photonic SHE is inaccurate if one of the conditions is not satisfied. Next, we consider the theory of weak measurements to observe the photonic SHE in atomically thin crystals without approximation. In our experiment, the preselected state is selected as $|H\rangle$, and the wave vector k_x

should be considered to accurately describe the behavior of the light beam. The state in Eq. (B2) with the reflection coefficient r_p being expanded as a Taylor-series expansion to the first order becomes

$$\begin{aligned} |k_{x,y}\rangle|H\rangle &\rightarrow |k_{x,y}\rangle|\varphi\rangle \\ &= |k_{x,y}\rangle \left[\left(r_p - \frac{k_x}{k_0} \frac{\partial r_p}{\partial \theta_i} \right) |H\rangle - k_y r_p \delta |V\rangle \right]. \end{aligned} \quad (\text{B6})$$

Far from the Brewster angle, the variation of k_x in the wave packet can be ignored and Eq. (B6) is approximated as $\exp(\mp k_y \delta)|\pm\rangle$ in the spin basis, as shown in the main text. This form can indicate clearly the interaction between the spin angular momentum and extrinsic orbital angular momentum of light in thin crystals.

To precisely obtain the separation of spin components, we next expand Eq. (B6) in the spin basis as

$$|\phi_{\pm}\rangle = |k_{x,y}\rangle \left[\left(r_p - \frac{k_x}{k_0} \frac{\partial r_p}{\partial \theta_i} \right) |\pm\rangle \pm i k_y r_p \delta |\pm\rangle \right]. \quad (\text{B7})$$

The reflection coefficients r_p and r_s in graphene are complex numbers, and we write them as $r_p = r'_p + i r''_p$ and $r_s = r'_s + i r''_s$. On the basis of Eq. (B7), the small shifts of the left-circularly-polarized and right-circularly-polarized components are calculated by $\langle \phi_{\pm}|y|\phi_{\pm}\rangle / \langle \phi_{\pm}|\phi_{\pm}\rangle$:

$$\delta_{\pm} = \mp \frac{2z_r r'_p (r'_p + r'_s) \cot \theta_i}{2k_0 z_r (r'^2_p + r'^2_s) + \xi^2}, \quad (\text{B8})$$

where $\xi = \text{Re}(\partial r_p / \partial \theta_i)$. Here $r''_p \ll 0$, and far from the Brewster angle, the contribution of ξ can be ignored. As a result, Eq. (B8) reduces to Eq. (5). We show the shifts with different optical conductivities $0.67\sigma_0$, σ_0 , and $1.33\sigma_0$ in Fig. 6. Increasing σ shifts the curve rightward. The angle indicated by the dotted black line is the angle of incidence to detect the photonic SHE in monolayer graphene. The change of the shift with the variation of $0.33\sigma_0$ is only about 0.5λ , which needs to be detected by the weak-measurement technique.

The weak value A_w in our case is purely imaginary and therefore we should consider the effective propagation distance z with a particular form of meter $\Phi(k_{x,y})$. If we take the free-flight Hamiltonian $H_{\text{free}} = -izk_y^2/2k_0$ into account, the meter state evolves as $\Phi(k_{x,y}) \rightarrow \Phi_z(k_{x,y}) = \Phi(k_{x,y}) \exp[-i(k_y^2/2k_0)z]$ [22,44]. So the total wavefunction state is described as

$$|\psi'\rangle = \int dk_x dk_y \Phi_z(k_{x,y}) |k_{x,y}\rangle |\varphi\rangle. \quad (\text{B9})$$

The preselected state $|\psi_i\rangle$ here is the pure polarization state $|H\rangle$. On the basis of the theory of weak measurements,

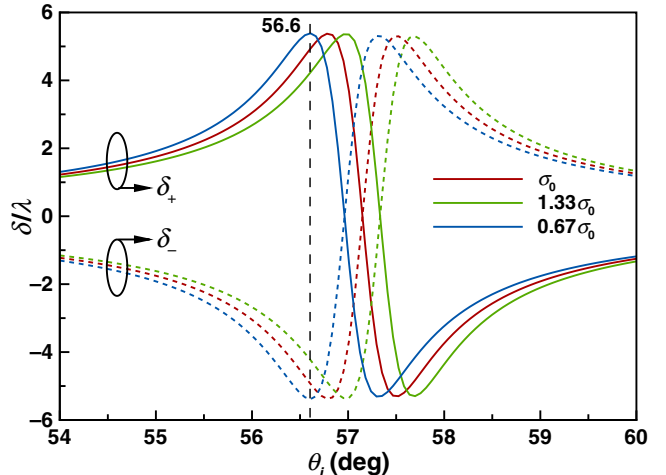


FIG. 6. Separation of spin components induced by the photonic SHE in graphene.

we postselect a nearly orthogonal state $|\psi_f\rangle = |V + \beta\rangle$ to obtain a purely imaginary weak value, in which β is referred to as the “postselected angle.” That is,

$$|\psi_i\rangle = |H\rangle, \quad (\text{B10})$$

$$|\psi_f\rangle = \sin(-\beta)|H\rangle + \cos\beta|V\rangle. \quad (\text{B11})$$

Subsequently, if we combine Eqs. (B11) and (B9), the final meter state becomes

$$\begin{aligned} |\phi\rangle &= \langle\psi_f|\psi'\rangle = \int dk_x dk_y \Phi_z(k_{x,y}) |k_{x,y}\rangle \\ &\times \left[\left(\frac{k_x}{k_0} \frac{\partial r_p}{\partial \theta_i} - r_p \right) \sin \beta - k_y r_p \delta \cos \beta \right]. \end{aligned} \quad (\text{B12})$$

The expectation value of the pointer observable y , also referred to as the “modified amplified pointer shift,” is obtained as

$$\begin{aligned} \langle y \rangle &= \frac{\langle \phi | y | \phi \rangle}{\langle \phi | \phi \rangle} \\ &= \frac{z r_p (r'_p + r'_s) \cot \theta_i \sin 2\beta}{(r'_p + r'_s)^2 \cos^2 \beta \cot^2 \theta_i + [2k_0 z_r (r'^2_p + r'^2_s) + \xi^2] \sin^2 \beta}. \end{aligned} \quad (\text{B13})$$

In our case, the reflection coefficient is almost real ($r''_p \ll 0$), and the first term in the denominator of Eq. (B13) can be ignored with $|r_p| \gg 0$. By doing so, we find that Eq. (B13) reduces to Eq. (5).

APPENDIX C: EXPERIMENTAL DATA FOR THE GRAPHENE SAMPLES

The circularly polarized components in the photonic SHE separate from each other by a tiny distance. The

light still exhibits a Gaussian profile when being reflected from graphene. However, after the procedure of weak measurements, these two spin components interfere with each other and the shape of the whole light beam undergoes an enhancement displacement. The intensity simulated from Eq. (B12) indicates the pointer shift of the centroid of the light beam. This enhancement displacement varies sensitively with the optical conductivity of graphene, which helps in accurate measurement of optical conductivity in our work.

In the experiment, the measurement of the optical conductivities of multilayer graphene is also considered. The pseudo-Brewster-angle increases with the number of layers of graphene, and the photonic SHE near the pseudo-Brewster-angle experiences strong spin-orbit interaction of light. Therefore, we choose the angles of incidence as 57.37° and 57.77° for bilayer graphene and trilayer graphene, respectively. Under this condition, there are two

advantages: (i) the optical conductivity of graphene is more sensitive to the amplified shift; (ii) at large β , the pointer shift can also be clearly distinguishable for various values of the conductivity. The data with larger β are more effective and stabler to determine the optical conductivity. The enhancement displacements of bilayer graphene and trilayer graphene with experimental data are given in Fig. 7. We assume that each individual graphene sheet is a noninteracting monolayer. The surface susceptibility χ is given by $n \times 8 \times 10^{-9}$ m, where n is the number of layers of graphene. We detect three groups of data for each sample at three different places. The theoretical curves in Fig. 7 are calculated by our considering the optical conductivity with a value of $n \times \sigma_0$. On the basis of these experimental results, the optical conductivities for the samples of bilayer and trilayer graphene are given in Fig. 5.

To confirm the samples we use are monolayer, bilayer, and trilayer graphene, we measure their Raman spectra with the Raman peak in the corresponding region of the prisms. The Raman spectra are shown in Fig. 8. For the few-layer-graphene samples, it is not obvious from the Raman spectra whether the samples have twist angles. The photonic SHE in bilayer graphene with various twist angles has been studied theoretically. It was shown that the splitting induced by the photonic SHE may be very different for the case of a twisted bilayer [43]. The conductivity of twisted-bilayer graphene at a wavelength of 633 nm (2.978×10^{15} rad/s) is obviously not equal to $2\sigma_0$ or even very large for a twist angle near 46.83° . Besides, the existence of diagonal components in the conductivity of twisted graphene can lead to a spin-dependent shift in the longitudinal direction for the photonic SHE [30,45]. In our experiment, however, we do not observe the related longitudinal shift in the photonic SHE, and the measured

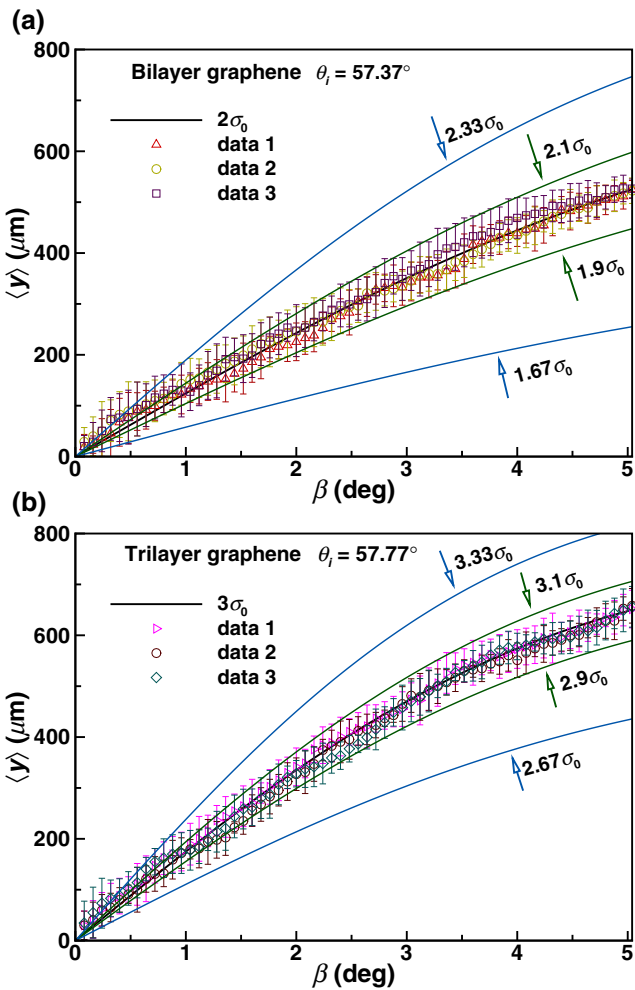


FIG. 7. Amplified splitting as a function of the angle β for samples of (a) bilayer graphene and (b) trilayer graphene. The solid lines indicate the theoretical results. We also detect three groups of data for each sample.

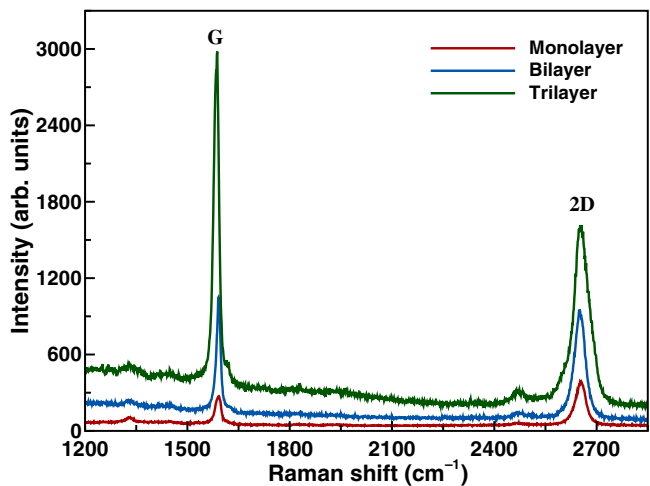


FIG. 8. Raman spectra of the samples to identify the region containing monolayer, bilayer, and trilayer graphene. G and 2D denote the Raman peaks originating from first-order and second-order Raman scattering processes in graphene, respectively.

shift is consistent with the simulation for conductivity of $2\sigma_0$ or $3\sigma_0$. Therefore, we infer that the graphene samples we use are not twisted. Our approach may be applied to measure the optical conductivity of few-layer graphene with a twist.

-
- [1] F. Bonaccorso, Z. Sun, T. Hasan, and A. C. Ferrari, Graphene photonics and optoelectronics, *Nat. Photonics* **4**, 611 (2010).
 - [2] K. S. Novoselov, A. K. Geim, S. V. Morozov, D. Jiang, Y. Zhang, S. V. Dubonos, I. V. Grigorieva, and A. A. Firsov, Electric field effect in atomically thin carbon films, *Science* **306**, 666 (2004).
 - [3] L. A. Falkovsky, Optical properties of graphene, *J. Phys.: Conf. Ser.* **129**, 012004 (2008).
 - [4] V. P. Gusynin, S. G. Sharapov, and J. P. Carbotte, Unusual Microwave Response of Dirac Quasiparticles in Graphene, *Phys. Rev. Lett.* **96**, 256802 (2006).
 - [5] T. Low, F. Guinea, H. Yan, F. Xia, and P. Avouris, Novel Midinfrared Plasmonic Properties of Bilayer Graphene, *Phys. Rev. Lett.* **112**, 116801 (2014).
 - [6] L. A. Falkovsky and A. A. Varlamov, Space-time dispersion of graphene conductivity, *Eur. Phys. J. B* **56**, 284 (2007).
 - [7] A. B. Kuzmenko, E. van Heumen, F. Carbone, and D. van der Marel, Universal Optical Conductance of Graphite, *Phys. Rev. Lett.* **100**, 117401 (2008).
 - [8] K. Ziegler, Minimal conductivity of graphene: Nonuniversal values from the Kubo formula, *Phys. Rev. B* **75**, 233407 (2007).
 - [9] T. Stauber, N. M. R. Peres, and A. K. Geim, Optical conductivity of graphene in the visible region of the spectrum, *Phys. Rev. B* **78**, 085432 (2008).
 - [10] R. R. Nair, P. Blake, A. N. Grigorenko, K. S. Novoselov, T. J. Booth, T. Stauber, N. M. R. Peres, and A. K. Geim, Fine structure constant defines visual transparency of graphene, *Science* **320**, 1308 (2008).
 - [11] K. F. Mak, M. Y. Sfeir, Y. Wu, C. H. Lui, J. A. Misewich, and T. F. Heinz, Measurement of the Optical Conductivity of Graphene, *Phys. Rev. Lett.* **101**, 196405 (2008).
 - [12] J. M. Dawlaty, S. Shivaraman, J. Strait, P. George, M. Chandrashekhar, F. Rana, M. G. Spencer, D. Veksler, and Y. Chen, Measurement of the optical absorption spectra of epitaxial graphene from terahertz to visible, *Appl. Phys. Lett.* **93**, 131905 (2008).
 - [13] K. F. Mak, J. Shan, and T. F. Heinz, Seeing Many-Body Effects in Single-and Few-Layer Graphene: Observation of Two-Dimensional Saddle-Point Excitons, *Phys. Rev. Lett.* **106**, 046401 (2011).
 - [14] M. Onoda, S. Murakami, and N. Nagaosa, Hall Effect of Light, *Phys. Rev. Lett.* **93**, 083901 (2004).
 - [15] K. Y. Bliokh and Y. P. Bliokh, Conservation of Angular Momentum, Transverse Shift, and Spin Hall Effect in Reflection and Refraction of an Electromagnetic Wave Packet, *Phys. Rev. Lett.* **96**, 073903 (2006).
 - [16] X. Yin, Z. Ye, J. Rho, Y. Wang, and X. Zhang, Photonic spin Hall effect at metasurfaces, *Science* **339**, 1405 (2013).
 - [17] N. Shitrit, I. Yulevich, E. Maguid, D. Ozeri, D. Veksler, V. Kleiner, and E. Hasman, Spin-optical metamaterial route to spin-controlled photonics, *Science* **340**, 724 (2013).
 - [18] K. Y. Bliokh, F. J. Rodríguez-Fortuño, F. Nori, and A. V. Zayats, Spin-corbit interactions of light, *Nat. Photonics* **9**, 796 (2015).
 - [19] X. Ling, X. Zhou, K. Huang, Y. Liu, C.-W. Qiu, H. Luo, and S. Wen, Recent advances in the spin Hall effect of light, *Rep. Prog. Phys.* **80**, 066401 (2017).
 - [20] X. Zhou, Z. Xiao, H. Luo, and S. Wen, Experimental observation of the spin Hall effect of light on a nanometal film via weak measurements, *Phys. Rev. A* **85**, 043809 (2012).
 - [21] Y. Aharonov, D. Z. Albert, and L. Vaidman, How the Result of a Measurement of a Component of the Spin of a Spin-1/2 Particle Can Turn Out to be 100, *Phys. Rev. Lett.* **60**, 1351 (1988).
 - [22] O. Hosten and P. Kwiat, Observation of the spin Hall effect of light via weak measurements, *Science* **319**, 787 (2008).
 - [23] P. Blake, E. W. Hill, A. H. Castro Neto, K. S. Novoselov, D. Jiang, R. Yang, T. J. Booth, and A. K. Geim, Making graphene visible, *Appl. Phys. Lett.* **91**, 063124 (2007).
 - [24] M. Bruna and S. Borini, Optical constants of graphene layers in the visible range, *Appl. Phys. Lett.* **94**, 031901 (2009).
 - [25] X. Zhou, X. Ling, H. Luo, and S. Wen, Identifying graphene layers via spin Hall effect of light, *Appl. Phys. Lett.* **101**, 251602 (2012).
 - [26] S. Chen, C. Mi, L. Cai, M. Liu, H. Luo, and S. Wen, Goos-Hänchen shift in graphene via weak measurements, *Appl. Phys. Lett.* **110**, 031105 (2017).
 - [27] M. Merano, Fresnel coefficients of a two-dimensional atomic crystal, *Phys. Rev. A* **93**, 013832 (2016).
 - [28] W. J. M. Kort-Kamp, B. Amorim, G. Bastos, F. A. Pinheiro, F. S. S. Rosa, N. M. R. Peres, and C. Farina, Active magneto-optical control of spontaneous emission in graphene, *Phys. Rev. B* **92**, 205415 (2015).
 - [29] M. Merano, Optical beam shifts in graphene and single-layer boron-nitride, *Opt. Lett.* **41**, 5780 (2016).
 - [30] L. Cai, M. Liu, S. Chen, Y. Liu, W. Shu, H. Luo, and S. Wen, Quantized photonic spin Hall effect in graphene, *Phys. Rev. A* **95**, 013809 (2017).
 - [31] A. G. Kofman, S. Ashhab, and F. Nori, Nonperturbative theory of weak pre- and postselected measurements, *Phys. Rep.* **520**, 43 (2012).
 - [32] J. Dressel, M. Malik, F. M. Miatto, A. N. Jordan, and R. W. Boyd, Colloquium: Understanding quantum weak values: Basics and applications, *Rev. Mod. Phys.* **86**, 307 (2014).
 - [33] X.-Y. Xu, Y. Kedem, K. Sun, L. Vaidman, C.-F. Li, and G.-C. Guo, Phase Estimation With Weak Measurement Using a White Light Source, *Phys. Rev. Lett.* **111**, 033604 (2013).
 - [34] A. N. Jordan, J. Martínez-Rincón, and J. C. Howell, Technical Advantages for Weak-Value Amplification: When Less is More, *Phys. Rev. X* **4**, 011031 (2014).
 - [35] A. Aiello and J. P. Woerdman, Role of beam propagation in Goos-Hänchen and Imbert-Fedorov shifts, *Opt. Lett.* **33**, 1437 (2008).
 - [36] S. Chen, C. Mi, W. Wu, W. Zhang, W. Shu, H. Luo, and S. Wen, Weak-value amplification for Weyl-point separation in momentum space, *New J. Phys.* **20**, 103050 (2018).

- [37] M. Liu, L. Cai, S. Chen, Y. Liu, H. Luo, and S. Wen, Strong spin-orbit interaction of light on the surface of atomically thin crystals, *Phys. Rev. A* **95**, 063827 (2017).
- [38] V. G. Kravets, A. N. Grigorenko, R. R. Nair, P. Blake, S. Anissimova, K. S. Novoselov, and A. K. Geim, Spectroscopic ellipsometry of graphene and an exciton-shifted van Hove peak in absorption, *Phys. Rev. B* **81**, 155413 (2010).
- [39] S. A. Mikhailov and K. Ziegler, New Electromagnetic Mode in Graphene, *Phys. Rev. Lett.* **99**, 016803 (2007).
- [40] S. Tebera and A. V. Kotikov, Field theoretic renormalization study of interaction corrections to the universal ac conductivity of graphene, *J. High Energy Phys.* **7**, 82 (2018).
- [41] C.-J. Kim, A. Sánchez-Castillo, Z. Ziegler, Y. Ogawa, C. Noguez, and J. Park, Chiral atomically thin films, *Nat. Nanotechnol.* **11**, 520 (2016).
- [42] Y. Cao, V. Fatemi, S. Fang, K. Watanabe, T. Taniguchi, E. Kaxiras, and P. Jarillo-Herrero, Unconventional superconductivity in magic-angle graphene superlattices, *Nature (London)* **556**, 43 (2018).
- [43] W. J. M. Kort-Kamp, F. J. Culchac, R. B. Capaz, and F. A. Pinheiro, Photonic spin Hall effect in bilayer graphene Moiré superlattices, *Phys. Rev. B* **98**, 195431 (2018).
- [44] S. Chen, X. Zhou, C. Mi, H. Luo, and S. Wen, Modified weak measurements for the detection of the photonic spin Hall effect, *Phys. Rev. A* **91**, 062105 (2015).
- [45] Z. Addison, J. Park, and E. J. Mele, Twist, slip, and circular dichroism in bilayer graphene, *Phys. Rev. B* **100**, 125418 (2019).